

MRI Compatibility and Visibility Assessment of Implantable Medical Devices

Beth A. Schueler, PhD,^{1*} Todd B. Parrish, PhD,² Jyh-Cherng Lin, PhD,³
Bruce E. Hammer, PhD,³ Brian J. Pangrle, PhD,⁴ E. Russell Ritenour, PhD,³
John Kucharczyk, PhD,³ and Charles L. Truwit, MD³

We have developed a protocol to evaluate the magnetic resonance (MR) compatibility of implantable medical devices. The testing protocol consists of the evaluation of magnetic field-induced movement, electric current, heating, image distortion, and device operation. In addition, current induction is evaluated with a finite element analysis simulation technique that models the effect of radiofrequency fields on each device. The protocol has been applied to several implantable infusion pumps and neurostimulators with associated attachments. Experiments were performed using a 1.5-T whole-body MR system with parameters selected to approximate the intended clinical and worst case configuration. The devices exhibited moderate magnetic field-induced deflection and torque but had significant image artifacts. No heating was detected for any of the devices. Pump operation was halted in the magnetic field, but resumed after removed. Exposure to the magnetic field activated some of the neurostimulators. J. Magn. Reson. Imaging 1999;9:596-603.

© 1999 Wiley-Liss, Inc.

Index terms: safety; artifacts; implantable devices; infusion pump; neurostimulator; implantable pulse generator

THE FOOD AND DRUG ADMINISTRATION (FDA) requires labeling of MR scanners to indicate that the imaging procedure is contraindicated for patients who have electrically, magnetically, or mechanically activated implants. The restriction is necessary due to the potential for the scanner's electromagnetic field to interfere with the implanted device's normal operation. At present, patients prohibited from MR exams include those with internal cardiac pacemakers, cochlear im-

plants, neurostimulators, bone-growth stimulators, and implantable drug infusion pumps. These and similar active devices, as well as passive devices, may pose a risk of adverse effects including magnetically induced movement, current, and heating.

To evaluate the safety and effectiveness of both active and passive implantable medical devices, a standard testing protocol is needed. This protocol must evaluate hazards to the patient that may result when the device is placed in the MR environment. In addition, the performance of the device should be monitored during and after MR imaging. A standard testing protocol should help to identify areas of potential hazard and assist in guiding design modifications to produce implants that are both MR safe and compatible.

We describe a generalized protocol to evaluate the MR compatibility of implantable devices. The protocol included an evaluation of five major areas: device movement, image artifact production, device heating, electric current induction, and device operation. The proposed tests were based predominantly on experimental measurements in a clinical MR environment, using phantoms with relaxation times within the biological ranges and device configurations that approximate actual device placement on a patient. When direct measurement was difficult, computer modeling techniques were utilized to evaluate possible hazards. We describe testing procedures associated with the five areas and the application of this protocol to implantable infusion pumps and neurostimulators.

MATERIALS AND METHODS

General MR Compatibility Protocol

Device Movement

Two types of magnetic field-induced movement of a metallic device may occur: deflection (translational movement) and torque (rotational movement). Due to the nature of the deflection force and torque, it is possible to isolate each type of movement and measure its magnitude separately. Deflection occurs in a region where a spatial magnetic field gradient is present. The deflection force will increase with the magnitude of the gradient. Typically, spatial gradients are greatest near

¹Mayo Clinic, Department of Diagnostic Radiology, 200 First Street SW, Rochester, MN 55905 (B.A.S.)

²Northwestern MRI Facility, 441 East Ontario, Chicago, IL 60611 (T.B.P.)

³University of Minnesota Hospital and Clinic, Department of Radiology, 420 Delaware St. SE, Minneapolis, MN 55455 (B.E.H., J.L., E.R.R., J.K., C.L.T.)

⁴Peacock, Myers and Adams, 201 Third Street NW, Suite 1340, Albuquerque, NM 87125 (B.J.P.)

*Address reprint requests to: B.A.S., Department of Diagnostic Radiology, Mayo Clinic, 200 First Street SW, Rochester, MN 55905.

Contract grant sponsor: Medtronic Inc., Minneapolis, MN.

Presented at the ISMRM Advances in MR Safety and Compatibility Workshop, McLean, VA, June, 1996.

Received November 12, 1996; Accepted October 26, 1998.

© 1999 Wiley-Liss, Inc.

the magnet portal. In contrast, the magnitude of the magnetic torque is proportional to the magnetic field strength. As a result, the torque is largest at the center of the magnet bore where the field gradient is negligible.

Deflection force. Deflection force was measured using a method initially described by New et al (1). The device was suspended on a silk suture attached at the center of mass and placed in the region near the magnet portal. The location of the suspended device was adjusted so that the angle of deflection from the vertical was greatest and the device remained at a height where the magnetic field gradient was horizontal. The angle of deflection was then measured with a protractor. The magnitude of the deflection force is

$$F = mg \tan \theta,$$

where m is the mass of the device, g is 9.8 m/s^2 , and θ is the deflection angle from vertical. For objects that have a deflection force much larger than their weight, the angle of deflection approached 90° . In this case, non-magnetic weights were attached to the device to make the deflection angle approximately 45° to improve measurement accuracy. The deflection force was then calculated from the sum of the device mass and the attached mass.

Torque. The method for measurement of torque has also been described by New et al (1). The device was suspended by one end using a silk suture and positioned at the center of the magnet bore. If the free end rotated to align with the magnetic field, the amount of torque was measured by attaching a lead weight to the free end. The weight was adjusted until the angle of rotation was 45° . The torque is given by

$$N = (M + m)Lg \sin \theta,$$

where M is the mass of the added weight, m is the mass of the device, L is the distance from the pivot to the center of mass (device + weight), g is 9.8 m/s^2 , and θ is the angle of rotation (45°).

If the weight of the device was large enough to prevent alignment of the dipole axis with the magnetic field, the device was suspended from its center of mass instead of one end. The torque is then

$$N = Mlg \sin \theta,$$

where M is the mass of the added weight, l is the distance from the suspended weight to the center of mass, g is 9.8 m/s^2 , and θ is the angle of rotation (45°).

For devices with a disc-like shape and/or internal components, the preferred orientation of each device in the magnetic field was not immediately obvious. To determine the preferred orientation, these devices were suspended from their center of mass and allowed to align with the magnetic field.

Imaging Artifacts

The distortion of MR images by various materials is caused by disruption of the local magnetic field resulting in a change in the position-frequency relationship,

which is crucial for accurate image reconstruction. The degree of image distortion depends on the magnetic susceptibility, shape, orientation, and position of the device in the body, as well as the MR technique, specific pulse sequence, and strength of the static and gradient magnetic field. Artifacts are most typically seen as local or regional distortions of the image, as signal voids or as increased noise.

To determine the degree of image distortion caused by the device, it was positioned on a phantom that was filled with an appropriate fluid mixture ($1.25 \text{ g NiSO}_4 \cdot 6\text{H}_2\text{O}$ and 5 g NaCl in 1000 ml water) to approximate the radiofrequency (RF) loading in the coil used. The device and phantom were imaged with both a spin-echo (SE) and gradient-echo (GE) sequence. To reduce the acquisition time, a turbo spin-echo (TSE) sequence with an echo train length 3, a TR of 300 msec, and an effective TE of 35 msec was used instead of the standard SE. The TSE sequence was modified to reproduce the slice selection and readout gradient strengths used in a typical SE on our system. We verified that the artifacts generated from the modified TSE sequence were similar to those of the SE by subtracting images of a device that caused a significant distortion. The GE sequence used was fast low-angle shot (FLASH) with a TR of 32 msec, TE of 15 msec, and a flip angle of 30° .

Image quality was evaluated according to the following criteria: a) geometric distortion, b) susceptibility-induced artifact (measured in GE images), c) warping artifact, and d) bending, warping, or obliteration of image contours. For each criteria, images were graded according to the following scale (3): no artifact, 0; mild artifact, smaller than device, 1; moderate artifact, same size as device, 2; strong artifact, larger than device, 3; severe artifact, larger than device, 4.

Device Heating

Conductive implants, materials, or devices may experience heating by the induction of electromotive forces when subjected to gradient magnetic fields. In addition, heating may be induced by arcing effects, if the device is placed too close to another conductor and sufficient voltage is generated. To determine if the device experiences a temperature increase, the device was placed within the magnet bore in various positions to approximate expected clinical orientations and worst-case heating conditions (ie, adjacent to the RF coil, oriented in all three directions relative to the z-axis of the magnet bore.) Temperature changes in the device were monitored with a fluoroptic probe (model 790, Luxtron, Santa Clara, CA) continually for 30 minutes. The temperature probe was capable of measuring temperature changes of $\pm 0.1^\circ\text{C}$. The imaging components of the pulse sequence were removed to increase the RF duty cycle. Both the TR and number of slices were adjusted to maximize the calculated specific absorption rate (SAR) without exceeding the FDA safe RF exposure recommendation (0.4 W/kg whole-body-averaged SAR). The heating sequence was then repeated with the device placed in a saline bath.

Induced Electric Current

Electric currents can be induced in metallic objects exposed to time-varying magnetic fields. Direct measurement of induced currents is difficult since introduction of a monitoring lead may change current paths. Instead of direct measurements, we assessed electromagnetic induced effects using a three-dimensional (3D) time-harmonic equation modeling package (FARADAY, Integrated Engineering, Winnipeg, Manitoba, Canada). The 3D time-harmonic solver models geometric volumes and their boundary interfaces. The program uses Maxwell's equations together with the appropriate boundary conditions to produce a set of equations in integral form. These equations are solved to yield the unknown field distribution, which includes localized eddy current formulations. Eddy currents on the surface of the conductor are due to the absorption of electromagnetic radiation; these result in a power loss that may be converted to heat and/or current discharge.

To impose a time-varying magnetic field over the sample, we utilized an eight-element birdcage resonator design. A cosine distribution current density was accomplished through the use of discrete wires on the surface of a cylinder. This model yielded a linearly polarized B_1 field that is orthogonal to B_0 (the static magnetic field). Using a linearly polarized field versus a circularly polarized field represented a worst-case scenario. The device of interest was modeled by assigning material properties (permeability, conductivity) and a discretized boundary element mesh. The synthesized object was inserted into the RF coil's center. A time-dependent current (frequency) was imposed on each birdcage wire to generate the B_1 fields varying from DC to 64 MHz. Depending on the current distribution through the birdcage elements, B_1 may be specified as a spatially uniform field or a linear field gradient in the transverse plane. Next, eddy current and magnetic field disturbances were calculated.

Device Operation

Active implantable devices containing components that are sensitive to the MR imaging environment can potentially experience alterations in operation. A device may be activated or deactivated when exposed to the static magnetic field, gradients or RF within the magnet bore or in the region surrounding the magnet. Preprogrammed instructions stored in programmable devices can also be altered or erased. Possible effects on device operation were assessed by monitoring device output during introduction to the static magnetic field, during imaging sequences, and after removal.

Applications

The general MR-compatibility protocol described above has been applied to two types of implantable devices: infusion pumps and neurostimulators (all devices from Medtronic, Minneapolis, MN).

The implantable infusion pump includes a self-contained case with a drug reservoir, a tiny peristaltic pump, and an energy source to drive the pump. Two SynchroMed pump models were tested: model 8611H

and model 8615, which incorporates an additional catheter access port. The programmable pumps contain electronics, valves, and solenoids, an antenna for communicating with an external programming unit, and a battery power source. The device can be programmed to deliver fluid by continuous infusion, timed boluses, or a combined pattern. A drug delivery catheter (model 8703W InDura) that attaches to the pump was also tested. The catheter includes silicone rubber proximal and distal sections with a titanium tubing connector. The distal section contains small tantalum markers at 1 cm increments for radiographic visibility.

The neurostimulator is an implantable pulse generator capable of providing pulses of variable voltage amplitude, pulsewidth, and rate. Attachments include several types of electrode combinations for stimulation of the spinal cord, brain, or peripheral nerves. Several models were tested: implantable pulse generators (model 7424 Itrel II and model 7425 Itrel III), receivers (model 3470 Xtrel Receiver and model 3272 Matrix Receiver), extensions, and leads (model 3888 Quad Plus Epidural Lead with model 7495 Extension; model 3387 Deep Brain Stimulation Lead, model 3586 Resume Epidural Lead and model 3898 Octapolar Epidural Lead with model 7496 Extension). The Itrel II and Itrel III pulse generators are active devices with an internal battery and circuitry enclosed in a titanium shield. The devices are provided with console and patient programmers and a control magnet that can be applied over the implanted device to switch it on and off or change between normal and low amplitude modes. The Xtrel and Matrix receivers are passive devices encased in epoxy-containing pulse-shaping circuitry to translate RF waves from an external transmitter and antenna into capacitor-coupled pulses. It is not expected that the transmitter and antenna will be placed in the MR environment and therefore they were not tested for MR compatibility. The leads include electrodes made of platinum and iridium, insulated with silicone rubber or polyurethane. Extensions and leads are variable lengths ranging from 10 to 80 cm.

Tests of these devices were performed on a Magnetom SP 1.5-T VISION whole-body, superconducting, actively shielded magnetic resonance imager (Siemens Medical Imaging Systems, Iselin, NJ). This MR system is equipped with a circularly polarized transmit/receive body and head coil. The RF power amplifier is capable of 12 kW in the body mode and 2 kW in the head mode. The peak amplitude of the gradient system on the scanner is 25 mT/m, and it is capable of ramping to peak in 600 μ sec. This results in a dB/dT of 42 T/m/sec.

RESULTS

Device Movement

Deflection Force

In the region surrounding the portal, both inside and outside the magnet bore, the magnetic field direction was determined with a magnaprobe (Cochranes, Oxford, England), and the magnitude of field strength was measured using a Hall probe (Walker Scientific, Worcester, MA). The measurements indicated that a horizontal magnetic field gradient exists along the center line of the

magnet bore. The location of maximum gradient along the center line was 16–18 cm from the portal, within the magnet bore. At this location, the magnetic field gradient was 230–250 gauss/cm, and the magnetic field strength was 9–10 kgauss.

The position of the suspended device was varied along the center line of the bore until the location of the maximum deflection angle was determined. For all the objects tested, this location was in the approximate region where the product of the magnetic field gradient and the magnetic field was largest. Each measurement was repeated five times and the results averaged. Table 1 lists the mass, deflection force, and force relative to the weight for each of the objects tested. Reproducibility was studied by performing a series of five measurements under similar conditions. These measurements indicated that the error in the force values was approximately $\pm 10\%$. No deflection force was detected for the catheter or any of the extensions or leads. Note that the maximum deflection force for the pumps and Itrel stimulators was less than the force of gravity. The Xtrel and Matrix receiver, however, deflected with a force larger than their weight. Additional non-magnetic weights were included in the receiver force measurement to adjust the deflection angle to approximately 45° .

Torque

Torque was measured at the center of the magnet bore. Results are listed in Table 2. The error in the torque values is approximately $\pm 20\%$, as estimated by performing multiple measurements under similar conditions. The last column of the table includes a ratio of the measured torque to N_{\max} , the maximum torque on the device produced by gravity, assuming that one edge of the device is fixed:

$$N_{\max} = mgD,$$

where m is the mass of the device, D is the maximum diameter, and g is 9.8 m/s^2 .

For the pumps and Itrel stimulators, the torque was found to be relatively weak, with all torque values less than the maximum gravitational torque expected. As a result, measurements were made with the devices suspended from their center of mass and the added weight suspended from one end of the alignment axis. For the Xtrel and Matrix receivers, the devices were suspended from one end of the axis with added weights suspended at the other end of the axis. In this case, the devices experienced a torque that was much larger, and the measurement technique could only estimate a lower

Table 1
Magnetic Field-Induced Deflection Force

Device	Mass (g)	Force (N)	Force/weight
Model 8611H SynchroMed Pump	203	1.1	0.55
Model 8615 SynchroMed Pump	217	1.4	0.66
Model 7424 Itrel II stimulator	45	0.32	0.73
Model 7425 Itrel III stimulator	42	0.17	0.41
Model 3470 Xtrel receiver	29	2.5	1.3
Model 3272 Matrix receiver	41	2.4	1.2

Table 2
Magnetic Field-Induced Torque

Device	Mass (g)	Torque ($N\cdot m \times 10^{-3}$)	Torque/ N_{\max}^a
Model 8611H SynchroMed Pump	203	28	0.20
Model 8615 SynchroMed Pump	217	29	0.19
Model 7424 Itrel II stimulator	45	23	0.87
Model 7425 Itrel III stimulator	42	20	0.93
Model 3470 Xtrel receiver	29	>70	>4
Model 3232 Matrix receiver	41	>70	>3

^a N_{\max} = maximum gravitational torque.

limit of its value. No torque was detected for the catheter or any of the extensions or leads.

Imaging Artifacts

Images of the pumps and neurostimulators were acquired with the device resting on an oval-shaped shoulder phantom using the body coil. A schematic of the set-up is shown in Fig. 1. Image artifacts are summarized in Table 3. Figure 2 shows Model 8611H SynchroMed pump, and Figs. 3 and 4 show the Itrel II pulse generator and Xtrel receiver. Images of both pump models, Itrel pulse generator models, and receiver models were similar. For all devices and pulse sequences tested, the image artifacts were found to be much larger than the size of the device itself. For the TSE images, the images exhibit severe distortion and smears since signal is remapped within the image. For the GE images, susceptibility artifacts occur as large areas of signal loss. The Xtrel and Matrix receivers exhibited the most extreme artifact, with near obliteration of the phantom in the GE images.

Table 3
Image Artifacts*

Device	Geometric distortion	T2* artifact	Warping artifact	Image contours
Model 8611H SynchroMed Pump	3	3	3	3
Model 8615 SynchroMed Pump	3	3	3	3
Model 8703W InDura Intra-spinal Catheter	0	0	0	0
Model 7424 Itrel II stimulator	3	3	3	3
Model 7425 Itrel III stimulator	3	4	3	3
Model 3470 Xtrel receiver	3	4	3	3
Model 3272 Matrix receiver	4	4	3	3
Model 7495 Extension	3	3	3	3
Model 7496 Extension	3	3	3	3
Model 3888 Quad Plus Epidural Lead	0	0	0	0
Model 3387 Deep Brain Stimulation Lead	0	0	0	0
Model 3586 Resume Epidural Lead	0	0	0	0
Model 3898 Octapolar Epidural Lead	0	0	0	0

*0 = no artifact, 1 = mild artifact (smaller than device), 2 = moderate artifact (same size as device), 3 = strong artifact (larger than device), 4 = severe artifact (larger than device).

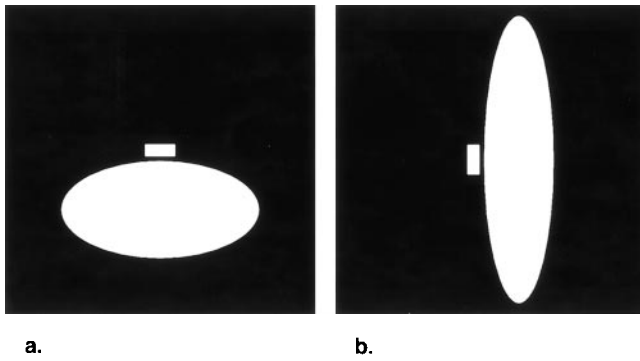


Figure 1. Schematic of device with phantom. **a:** Axial, field of view 30×30 cm. **b:** Sagittal, field of view 50×50 cm.

The catheter, extensions, and leads were connected to the corresponding devices and positioned along the center of the phantom. Images were then acquired at various points along the length of the catheter or wires, including the regions where connectors were located. Images of the phantom with the catheter and each of the leads demonstrated no image distortion, using both GE and TSE sequences. In addition, both extensions (models 7495 and 7496) showed no artifacts when imaged through the center of the wires. However, the extension-lead connectors caused artifacts in both GE and TSE images (Fig. 5), showing distorted images with areas larger than the size of connector (actual size: 5×15 mm). These observations imply that the image quality in the area where the leads are located would not be affected if the extensions and devices mentioned above were positioned far away from the region of interest.

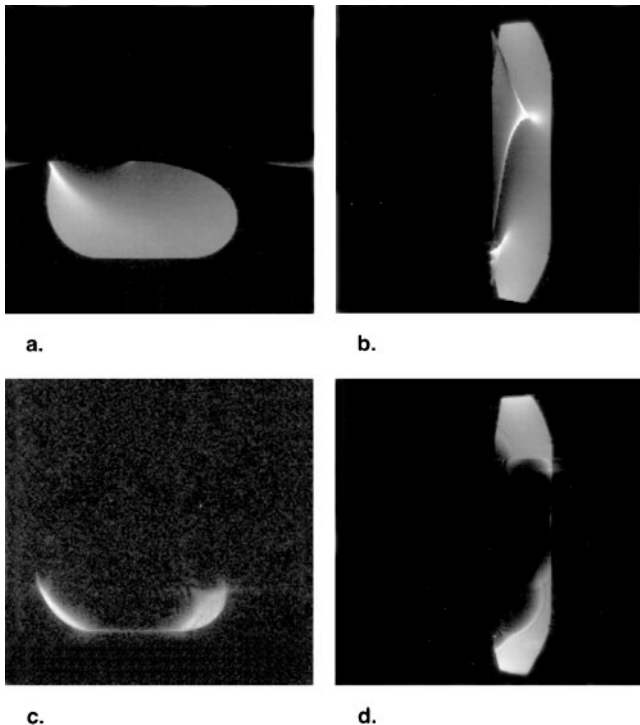


Figure 2. Model 8611H infusion pump with phantom. Slices are centered over the device. **a,b:** Axial and sagittal spin echo. **c,d:** Axial and sagittal gradient echo.

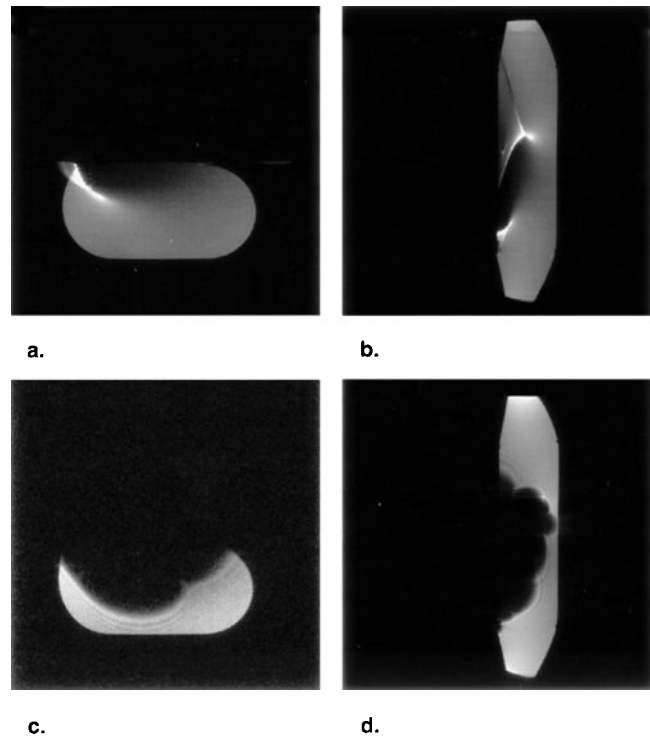


Figure 3. Model 7424 Itrel II implantable pulse generator with phantom. Slices are centered over the device. **a,b:** Axial and sagittal spin echo. **c,d:** Axial and sagittal gradient echo.

Device Heating

No heating of any of the devices, catheters, extensions, or leads was detected in several separate experiments in which the location and orientation of objects within the magnet bore were varied. Potential heating was also monitored with active devices programmed to deliver a fluid bolus or voltage pulse. No temperature rise was detected.

Induced Electric Current

To approximate a worst-case configuration, an object simulating the shape of an implantable pulse generator was modeled as a solid aluminum prolate spheroid ($6 \times 4 \times 1.5$ cm). The resulting magnetic field magnitude generated by the model is shown in Fig. 6, and the current density on the surface of the model is shown in Fig. 7. Eddy current density was found to increase with frequency. At 64 MHz, the current density maximum was 7×10^9 A/m². In addition, the current density was found to be largest at sharp edges and corners, as can be seen in Fig. 7.

Device Operation

To test device operation of the pump, the reservoir was filled with water and programmed to operate in periodic bolus delivery mode ($10 \mu\text{l}$ every 5 minutes). The performance of the pump was monitored outside of the magnet room, and then the device was placed inside the magnet. During the time period that the pump was inside the magnetic field, the bolus was not delivered. Bolus delivery resumed at the programmed delivery rate

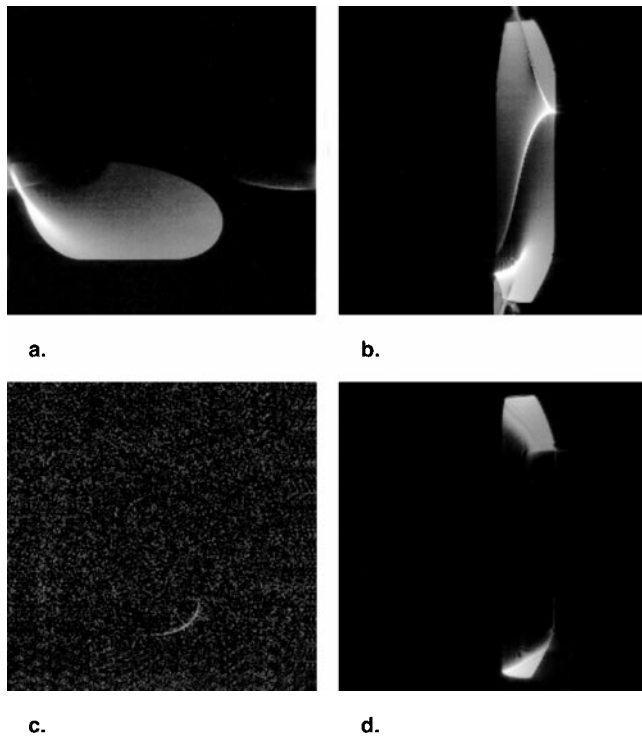


Figure 4. Model 3470 Xtrel receiver with phantom. Slices are centered over the device. a,b: Axial and sagittal spin echo. c,d: Axial and sagittal gradient echo.

after the pump was removed from the magnet. No effect on the operation of the pump was seen during or following multiple imaging sequences when the device was programmed for no fluid delivery. Subsequent reprogramming of the device for continuous infusion and timed boluses at a range of delivery rates was verified to be normal.

The operation of the active stimulators (Itrel II and Itrel III) was monitored by connecting a piezo-electric buzzer to the device to indicate when voltage pulses were generated. When introduced to the region surrounding the magnet bore, the stimulator was activated and deactivated as its orientation in the magnetic field changed. The activation status remained unchanged if the device was kept stationary. The status also remained unchanged during application of imaging sequences. Subsequent reprogramming of the device was verified to be normal. The operation of the stimulators was also tested after they had been programmed to generate a zero amplitude voltage pulse, which acts as another method of device deactivation. In this mode, no change in the device operation was detected during magnetic field exposure and imaging.

DISCUSSION

The safety and compatibility of various implantable medical devices in an MR environment has been examined in a number of previous studies. The components of the testing protocol presented here incorporate aspects of these previous studies and add some new analyses to develop a comprehensive evaluation scheme for active and passive devices. In general, it is difficult to

make universal statements about safety of a device given the high variability in the magnetic environment, equipment, implementation of technique, and application of the device.

Methods for measurement of magnetic field-induced movement have been presented by New et al (1) and have subsequently been applied to aneurysm clips, intravascular devices, dental implants, and other implanted devices or foreign objects (2–6). In general, the method of deflection force measurement has become well established. It should be noted that for some MR units, the maximum magnetic field gradient may be located near the corner of the solenoid windings instead of along the center line. In this case, the deflection force could be higher at this location. Although it is difficult to measure directly the force near the wall of the bore, the value can be calculated from the force measured along the center line, if the magnetic classification of the material is known. For “hard” magnetic (ferromagnetic) materials, which have a nonzero inherent magnetization and high magnetic susceptibility, the deflection force is proportional to the spatial magnetic field gradient. For “soft” magnetic (paramagnetic) materials, which are not magnetized unless they are placed in an external magnetic field, the force is proportional to the product of the magnetic field strength and the gradient (7). It is important to measure the spatial distribution of the magnetic field for the particular MR system being used to determine the location, direction, and magnitude of the maximum magnetic field gradient for that system.

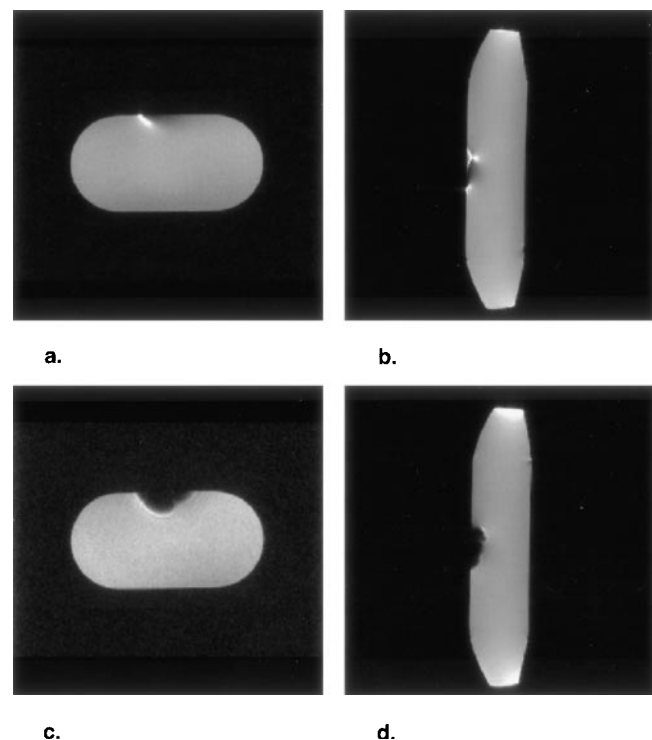


Figure 5. Model 7475 Extension with phantom. Slices are centered over the connection between the extension and lead. a,b: Axial and sagittal spin echo. c,d: Axial and sagittal gradient echo.

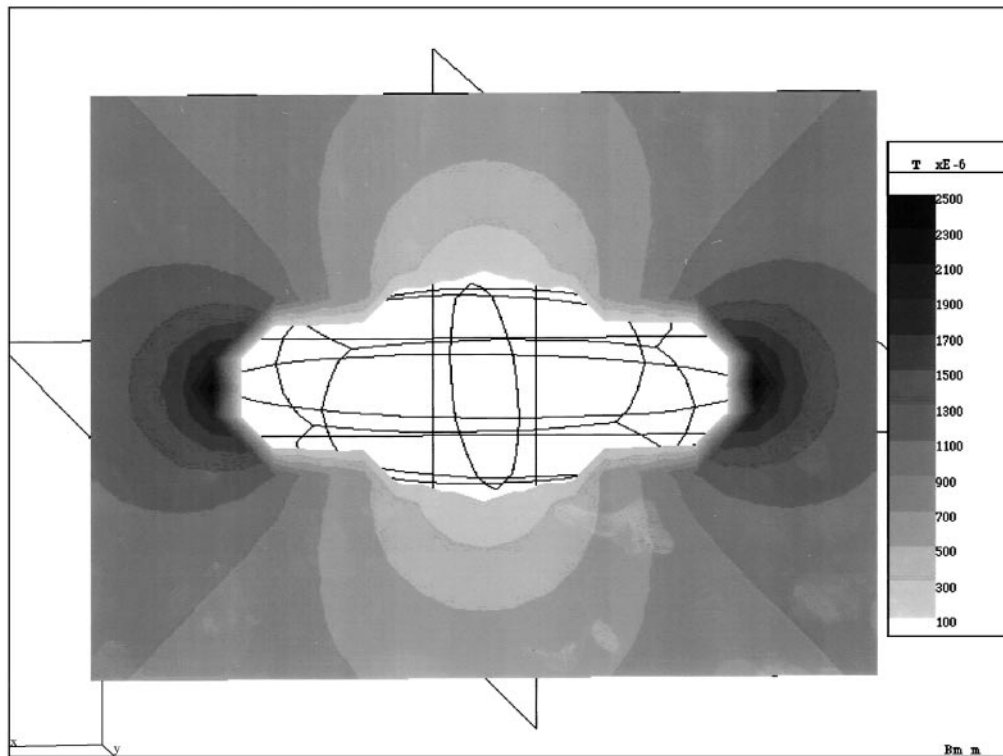


Figure 6. Magnetic field magnitude generated by the implantable pulse generator modeled as a solid aluminum prolate spheroid ($6 \times 4 \times 1.5$ cm). The magnetic field surrounding the device in the plane transverse to coil axis is shown.

The measurement of torque has been found to be more problematic, particularly for objects that do not exhibit a well-defined axis of alignment. An alternative measurement technique using a force/torque moment

transducer has been developed by Planert et al (8), which may provide more accurate results for complex objects than the method we have presented. Regardless, our results and data presented by Planert et al indicate

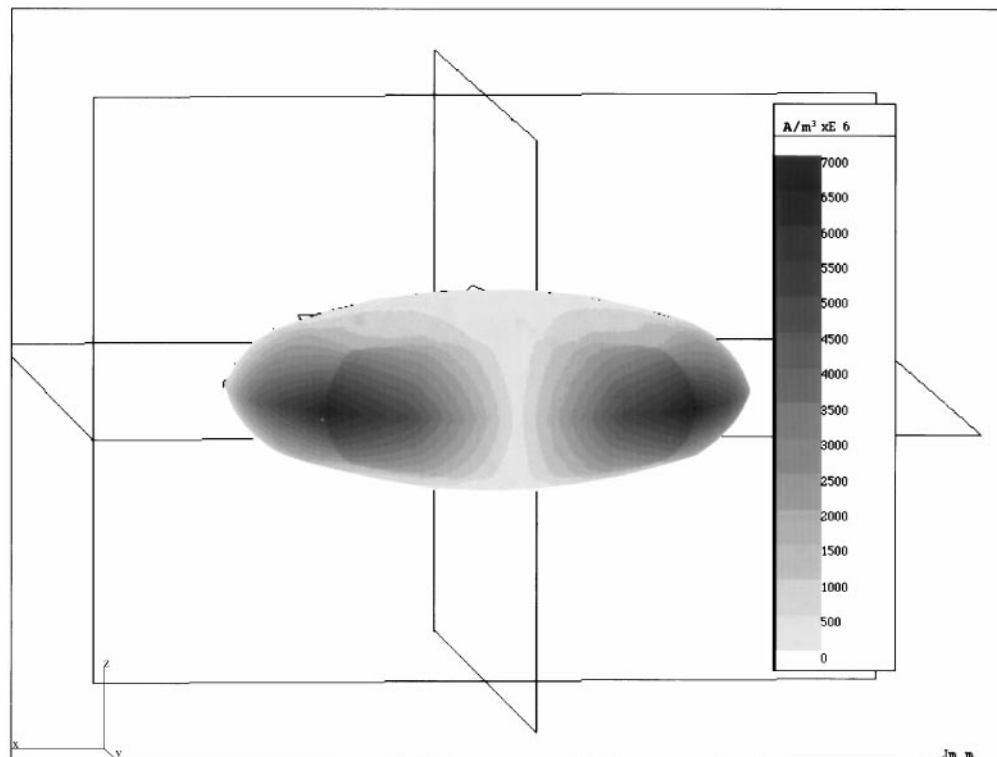


Figure 7. Eddy current density on the surface of the implantable pulse generator model.

that for magnetic field strength and gradients of a typical 1.5-T MR unit, an object with a large maximum deflection force will also have a large maximum torque.

Heating effects on objects implanted or in contact with the patient have been studied for a number of different medical devices. Davis et al (9) found no significant increase in temperature in metal surgical clips and prosthesis, except when two large hip prostheses were placed together in saline and exposed to RF fields. The latter result was believed to be due to the large conducting paths created when the two prostheses were in contact and surrounded by conducting solution. Further studies found no significant temperature increase in prosthetic heart valves (10). Buchli et al (11) conducted experimental studies and theoretical calculations showing that even large nonferromagnetic metallic implants will not experience a measurable temperature rise. Reports of focal heating and burns have been presented in the literature (12); these are believed to result from the formation of a conductive loop created by a electrode lead and the patient's skin. Further investigation of this effect for the case of conducting loops implanted in tissue or within blood vessels is needed.

Heating resulting from induced current in conducting devices has been studied by Buchli et al (11). However, the effect of induced current and voltage in devices implanted in electrically stimuable tissue has not been adequately studied. Pavlicek et al (13) estimated the potential voltage signal induced in a pacemaker during MR imaging and found it to be lower than the threshold required to stimulate cardiac activity. Other studies (14,15) have found that some pulse generators induce cardiac stimulation at a rate equal to the RF pulse period during in vivo testing. Neurostimulation is also a potential area of difficulty. Since direct measurement of electrical current in these circumstances was problematic, computer modeling of current distributions is necessary. In addition to device evaluation, computer models may also be useful for device design. For example, our simplified models have indicated that eddy currents can be reduced by using materials that possess a low conductivity and by having objects without sharp bends or corners. Further development of the current computer model is needed to simulate more accurately actual device shapes and multiple components.

ACKNOWLEDGMENTS

The authors thank Dennis E. Elsberry, DVM, PhD; Kenneth Heruth, MS; Mark Rise, PhD; and Brenda K. Schultz, RN, MBA for their technical assistance.

REFERENCES

1. New PJF, Rosen BJ, Brady TJ, et al. Potential hazards and artifacts of ferromagnetic and nonferromagnetic surgical and dental materials and devices in nuclear magnetic resonance imaging. *Radiology* 1983;147:139-148.
2. Teitelbaum GP, Bradley WG, Klein BD. MR imaging artifacts, ferromagnetism, and magnetic torque of intravascular filters, stents, and coils. *Radiology* 1988;166:657-664.
3. Shellock FG, Crues JV. High-field-strength MR imaging and metallic biomedical implants: an ex vivo evaluation of deflection forces. *AJR* 1988;151:389-392.
4. Shellock FG, Morisoli SM. Ex vivo evaluation of ferromagnetism, heating and artifacts produced by heart valve prostheses exposed to a 1.5-T MR system. *J Magn Reson Imaging* 1994;4:756-768.
5. Moscatel MA, Shellock FG, Morisoli SM. Biopsy needles and devices: assessment of ferromagnetism and artifacts during exposure to a 1.5 T MR system. *J Magn Reson Imaging* 1995;5:369-372.
6. Von Roemeling R, Lanning RM, Eames FA. MR imaging of patients with implanted drug infusion pumps. *J Magn Reson Imaging* 1991;1:77-81.
7. Schenk JF. The role of magnetic susceptibility in magnetic resonance imaging: MRI magnetic compatibility of the first and second kinds. *Med Phys* 1996;23:815-850.
8. Planert J, Modler H, Vosschenrich R. Measurements of magnetism-related forces and torque moments affecting medical instruments, implants, and foreign objects during magnetic resonance imaging at all degree of freedom. *Med Phys* 1996;23:851-856.
9. Davis PL, Crooks L, Arakawa M, McRee R, Kaufman L, Margulis AR. Potential hazards in NMR imaging: heating effects of changing magnetic fields and RF fields on small metallic implants. *AJR* 1981;137:857-860.
10. Soulen RL, Budinger TF, Higgins CB. Magnetic resonance imaging of prosthetic heart valves. *Radiology* 1985;154:705-707.
11. Buchli R, Boesiger P, Meier D. Heating effects on metallic implants by MRI examination. *Magn Reson Med* 1988;7:255-261.
12. Kanal E, Shellock FG, Talagala L. Safety considerations in MR imaging. *Radiology* 1990;176:593-606.
13. Pavlicek W, Geisinger M, Castle L, et al. The effects of nuclear magnetic resonance on patients with cardiac pacemakers. *Radiology* 1983;147:149-153.
14. Fetter J, Aram G, Holmes DR, Gray JE, Hayes DL. The effects of nuclear magnetic resonance imagers on external and implantable pulse generators. *PACE* 1984;7:720-727.
15. Holmes DR, Hayes DL, Gray JE, Meredith J. The effects of magnetic resonance imaging on implantable pulse generators. *PACE* 1986;9:360-370.